Intraseasonal versus Interannual Measures of Land–Atmosphere Coupling Strength in a Global Climate Model: GLACE-1 versus GLACE-CMIP5 Experiments in ACCESS1.3b

RUTH LORENZ, ANDREW J. PITMAN, AND ANNETTE L. HIRSCH

ARC Centre of Excellence for Climate System Science, and Climate Change Research Centre, University of New South Wales, Sydney, New South Wales, Australia

JHAN SRBINOVSKY

CSIRO Oceans and Atmosphere Flagship, Aspendale, Victoria, Australia

(Manuscript received 14 October 2014, in final form 20 March 2015)

ABSTRACT

Land–atmosphere coupling can strongly affect climate and climate extremes. Estimates of land–atmosphere coupling vary considerably between climate models, between different measures used to define coupling, and between the present and the future. The Australian Community Climate and Earth-System Simulator, version 1.3b (ACCESS1.3b), is used to derive and examine previously used measures of coupling strength. These include the GLACE-1 coupling measure derived on seasonal time scales; a similar measure defined using multiyear simulations; and four other measures of different complexity and data requirements, including measures that can be derived from standard model runs and observations. The ACCESS1.3b land–atmosphere coupling strength is comparable to other climate models. The coupling strength in the Southern Hemisphere summer is larger compared to the Northern Hemisphere summer and is dominated by a strong signal in the tropics and subtropics. The land–atmosphere coupling measures agree on the location of very strong land–atmosphere coupling but show differences in the spatial extent of these regions. However, the investigated measures show disagreement in weaker coupled regions, and some regions are only identified by a single measure as strongly coupled. In future projections the soil moisture trend is crucial in generating regions of strong land–atmosphere coupling, and the results suggest an expansion of coupling ''hot spots.'' It is concluded that great care needs to be taken in using different measures of coupling strength and shown that several measures that can be easily derived lead to inconsistent conclusions with more computationally expensive measures designed to measure coupling strength.

1. Introduction

The land surface and the atmosphere are linked by the exchange of water, energy, and trace gases (Seneviratne et al. 2010). Depending on the region and the climate, the land surface can amplify or dampen the fluxes and feedbacks associated with interactions between the land and the atmosphere. Air temperature, boundary layer stability, and in some cases precipitation are influenced by land–atmosphere interactions (e.g., Betts et al. 1996; Findell and Eltahir 2003; Seneviratne et al. 2010). For example, heat waves are influenced by soil moisture (SM) where dry conditions lead to an amplification of hot temperature anomalies (Fischer et al. 2007; Koster et al. 2009a; Hirschi et al. 2011; Mueller and Seneviratne 2012; Miralles et al. 2014). Since the land surface has a longer memory component than the atmosphere, land–atmosphere interactions also play a role in subseasonal forecasting, although any skill associated with land–atmosphere interactions is generally larger for temperature than precipitation (van den Hurk et al. 2012; Koster et al. 2011; Hirsch et al. 2014a). In Europe, the effect from soil moisture on air temperature is asymmetric. The influence associated with dry conditions leading to hotter temperatures is larger than the dampening of

Corresponding author address: Ruth Lorenz, ARC Centre of Excellence for Climate System Science, University of New South Wales, Level 4, Mathews Building, Sydney NSW 2052, Australia.
E-mail: r.lorenz@unsw.edu.au

DOI: 10.1175/JHM-D-14-0206.1

temperatures in wet conditions (Jaeger and Seneviratne 2011; Lorenz et al. 2012; Quesada et al. 2012). For Australia, it was shown that the influence of soil moisture on temperature is stronger for maximum compared to minimum temperatures (Hirsch et al. 2014b). Other studies suggest that feedbacks between the land surface and climate are a significant part of simulated changes in future climate projections (Seneviratne et al. 2006, 2013; Diffenbaugh and Ashfaq 2010; Boberg and Christensen 2012).

The terms ''land–atmosphere interactions,'' ''feedback,'' and ''coupling'' are often used interchangeably. We use these terms consistent with the definitions provided by Seneviratne et al. (2010). Coupling means the degree to which one variable controls another. For example, soil moisture–temperature coupling describes the degree to which soil moisture controls near-surface air temperature. As an extension, coupling can more generally refer to processes in one sphere (e.g., the land) influencing processes in another sphere (e.g., the atmosphere). A two-way coupling is a feedback, and interactions are more generally used without indicating direction. Hence, land–atmosphere coupling measures how strongly atmospheric processes are influenced by the anomalies in the land surface state, for example soil moisture. Land–atmosphere coupling is difficult to quantify (Koster et al. 2004, 2006; Wang et al. 2007; Orlowsky and Seneviratne 2010), and there are several ways to calculate a coupling measure. Most commonly, land–atmosphere coupling refers to a measure determined using climate model experiments where the land can be artificially decoupled from the atmosphere (Koster et al. 2002, 2006; Seneviratne et al. 2010). This is achieved by prescribing one or several land surface state variables, most commonly soil moisture, that remove one part of the land–atmosphere feedback. The coupling strength then compares the variance in the uncoupled and coupled model runs (see section 2d). By calculating the difference between coupled and uncoupled model experiments, the influence of the prescribed variable on land–atmosphere coupling can be quantified (Delworth and Manabe 1988; Koster et al. 2006; Seneviratne et al. 2006; Jaeger and Seneviratne 2011; Lorenz et al. 2012).

Koster et al. (2004, 2006) presented the first model intercomparison study focused on land–atmosphere coupling: the Global Land–Atmosphere Coupling Experiment (GLACE-1), where the coupling strength was quantified for a single boreal summer and global ''hot spots'' were identified. Wang et al. (2007) proposed an additional soil moisture–precipitation coupling measure and found a strong dependence of the GLACE-1 index on atmospheric internal variability to be a potential cause for the differences between the two indices. Guo and Dirmeyer (2013) extended the GLACE-1 framework to a multiyear experiment and found significant interannual variability (IAV) in land–atmosphere coupling strength for the boreal summer. Hirsch et al. (2014b) presented an estimate for land–atmosphere coupling strength in the austral summer. They showed an impact of soil moisture on maximum and mean temperature of the same order of magnitude as found in the Northern Hemisphere for boreal summer. Seneviratne et al. (2006) investigated land–climate coupling in climate change conditions, using a very similar measure to GLACE-1 to estimate coupling strength but focusing on temperature in Europe on interannual timescales.

Some land–atmosphere coupling measures do not require specialized simulations. Seneviratne et al. (2006) estimated soil moisture–temperature coupling using the correlation between evapotranspiration and temperature, which are available from typical multiyear climate model simulations. Miralles et al. (2012) proposed a soil moisture–temperature coupling measure Π as the difference in the correlation coefficients between temperature and energy based on observational data (see section 2d). This kind of correlation cannot demonstrate links of causality (Orlowsky and Seneviratne 2010; Seneviratne et al. 2010; Miralles et al. 2012), and therefore, according to our definition of land–atmosphere coupling, it can only indicate land–atmosphere interactions. Dirmeyer (2011) and Dirmeyer et al. (2014) split land–atmosphere coupling into two pathways: a terrestrial segment linking the state of the land to the surface fluxes and an atmospheric segment linking the surface fluxes to the state of the atmosphere. The first leg indicates the potential of the land surface to influence the atmosphere, so it is a necessary but not sufficient condition (Dirmeyer 2011). The second leg then adds the influence from the surface fluxes on the atmospheric state to the full land–atmosphere feedback. The last measure we examined, a quantile regression analysis, relates the number of hot days to the previous month's standard precipitation index (SPI), which is a proxy for soil moisture anomalies (Hirschi et al. 2011; Mueller and Seneviratne 2012). This estimates the influence of dry land surface conditions on temperature extremes and can be derived from temperature and precipitation observations.

We use the Australian Community Climate and Earth-System Simulator, version 1.3b (ACCESS1.3b), to conduct a GLACE-1 (Koster et al. 2006) experiment including 16 member ensembles (with different initial conditions) of 3-month-long model simulations, two ensembles for three summer seasons per hemisphere. For both hemispheres, for each year, we calculate one

ensemble where soil moisture is interactive and one where soil moisture is prescribed every time step (thereby decoupling the land from the atmosphere). We also run the GLACE-CMIP5-type experiment using prescribed soil moisture over the CMIP5 period to investigate the effects of changes in soil moisture content and soil moisture–climate coupling for future climate projections (Seneviratne et al. 2013). GLACE-CMIP5 focuses on two experiments: one where soil moisture is prescribed by the climatology from 1971 to 2000 from the control simulation with interactive soil moisture and one where soil moisture is prescribed by the transient climatology. We then compare several coupling measures derived from our GLACE-1 and GLACE-CMIP5 simulations and investigate ACCESS1.3b's coupling strength. We have several goals: first, we aim to document the coupling strength in ACCESS1.3b because this informs a range of future work with this model examining the role of land surface processes and feedbacks. We also seek to determine whether the model's coupling strength is anomalous in comparison with published estimates. Lorenz et al. (2014) evaluated ACCESS1.3b and showed that there were deficiencies with the simulation of daily minimum and maximum temperature. We examine whether these are linked with anomalous land–atmosphere coupling. Finally, and of most widespread interest, we demonstrate whether different methods of estimating coupling strength provide consistent conclusions. GLACE-1 and GLACE-CMIP5 are computationally demanding experiments, and measures of coupling strength have been proposed that avoid these costs by using generic simulations. We examine whether measures derived from these two approaches provide consistent results.

2. Methods

a. Model description

ACCESS is a state-of-the-art, fully coupled climate and weather prediction model (Puri et al. 2013). ACCESS1.3b consists of the atmospheric Unified Model (UM); the Community Atmosphere Biosphere Land Exchange (CABLE) land surface model; the Modular Ocean Model; and the Los Alamos Sea Ice Model (CICE; Bi et al. 2013). We used prescribed sea surface temperatures and sea ice and focus on the atmosphere and land components below.

The atmospheric model in ACCESS1.3b is UM, version 7.3 (Davies et al. 2005; Martin et al. 2006). Atmospheric dynamics are nonhydrostatic and fully compressible, and the advection scheme is semi-Lagrangian. The radiation scheme is a general two-stream scheme (Edwards and Slingo 1996; Hewitt et al. 2011). Convection is parameterized by a modified mass flux scheme (Gregory and Rowntree 1990). The convective available potential energy closure scheme is based on relative humidity, and convective momentum transport is parameterized for shallow and deep convection. The critical water content for precipitation is a function of cloud depth, and shallower clouds need higher water content before they start to generate precipitation.

The land surface model CABLE, version 2.0 (CABLE2.0), represents canopy processes via a one-layer, two-leaf canopy scheme for photosynthesis, stomatal conductance, and leaf temperature (Wang and Leuning 1998). CABLE distinguishes nine vegetation types and four nonvegetated types, using up to five tiles within each grid cell. The soil model has six layers and the Richards equation is solved for soil moisture while soil temperature is calculated from the heat conduction equation. The snow model has three snowpack layers and calculates temperature, density, and thickness of the snow. Further detailed descriptions of CABLE1.4 can be found in Wang et al. (2011), CABLE1.8 in Kowalczyk et al. (2013), and CABLE2.0 in Lorenz et al. (2014).

We use ACCESS1.3b in an Atmospheric Model Intercomparison Project (AMIP) configuration (Gates 1992) with prescribed sea surface temperatures and sea ice fractions. These were sourced from the Program for Climate Model Diagnosis and Intercomparison (Taylor et al. 2000; PCMDI 2013) for 1950–2006 and the ACCESS1.3 CMIP5 RCP8.5 run for 2007–2100 (Dix et al. 2013). We performed simulations at 1.25° latitude × 1.875° longitude resolution with 38 vertical levels and a 30-min time step. The simulations cover 1950–2100 for GLACE-CMIP5 and December–February (DJF) and June–August (JJA) for GLACE-1. We simulated three different years for GLACE-1: 1982/83, 1993/94, and 1999/2000. Results from two versions of ACCESS, submitted as part of CMIP5, suggest the model performs very well in comparison to other CMIP5 models (Flato et al. 2013). ACCESS1.3b has been evaluated by Lorenz et al. (2014) and was found to represent the global climate reasonably well, with some deficiencies in daily minimum and maximum temperature as well as evapotranspiration, similar to other CMIP5 models (e.g., Lewis and Karoly 2013; Mueller and Seneviratne 2014).

b. GLACE-1 experiments

The GLACE-1 experiment consists of two model ensembles. The first is a write ensemble, where soil moisture is calculated interactively and is different in every ensemble member (ensemble W). Soil moisture is written out at every time step from one ensemble

member (*W*1). In the second ensemble (ensemble *R*), soil moisture is identical in every ensemble member; the data from *W*1 is read back into the model and substitutes the soil moisture calculation. We run 16 members for each of the write ensembles and read ensembles as described in Koster et al. (2004, 2006). We prescribed soil moisture in the whole soil column, in contrast to Koster et al. (2004, 2006), where only subsurface soil moisture was prescribed, consistent with the design of GLACE-CMIP5 (see section 2c). In GLACE-1, the top soil layer was not prescribed to avoid effects from fast processes such as bare soil evaporation. This difference in methodologies needs to be kept in mind when comparing our GLACE-1 results to other studies. We run three different summers per hemisphere: 1982/83 (an El Niño year); 1993/94 (a neutral year), which was used in Koster et al. (2004, 2006) for the boreal summer; and 1999/2000 (a La Niña year).

The GLACE-1 ensembles were obtained by using different restart files from an earlier 60-yr simulation. For JJA, we use restart files from neutral years as described in Koster et al. (2006). We use years where the Niño-3 index anomaly prior to the restart date (1 June) was less than 0.5 based on CPC (2013a,b). For DJF the same criteria did not provide enough restart files, so we included some of the years used in JJA with small anomalies prior to 1 December, 3 years with a positive anomaly and 3 years with a negative anomaly. We run three seasons for DJF and JJA each: 1982/83, 1993/94, and 1999/2000. We chose these years following Koster et al. (2006), who used JJA 1994 as a neutral El Niño year, and Hirsch et al. (2014b), who used an El Niño year, 1982/83, and a La Niña year, 1999/2000, corresponding to dry and wet conditions over Australia.

c. *GLACE-CMIP5 experiments*

This experiment uses prescribed soil moisture experiments over the CMIP5 period to investigate the effects of changes in soil moisture content and soil moisture–climate coupling for future climate projections (Seneviratne et al. 2013). It focuses on two experiments: experiment A (ExpA), where soil moisture is prescribed by the climatology from 1971 to 2000 from the control simulation with interactive soil moisture, and experiment B (ExpB), where soil moisture is prescribed by the transient climatology (running means over 30-yr periods). The model version used was updated since CMIP5, and therefore, the reference run (CTL) is not exactly identical to CMIP5 but rather to a new AMIP run. Figure 1 shows the globally averaged soil moisture content in the ACCESS1.3b GLACE-CMIP5 runs. After writing the soil moisture data from the reference run, we

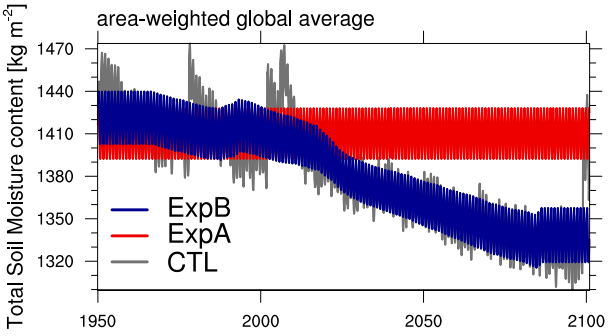

FIG. 1. Total soil moisture (kg m^{-2}) in ACCESS1.3b in the GLACE-CMIP5 experiments CTL, ExpA, and ExpB.

calculate climatologies. For the experiments, we then read in these soil moisture climatologies. The climatologies were calculated for every time step at every grid point.

GLACE-CMIP5 was designed to examine longer time scales (multidecadal) than the seasonal scales examined in GLACE-1, and the two experiments are complementary. Since we used observed sea surface temperatures and sea ice prior to 2007 and data modeled from CMIP5 thereafter, we compare the conditions at the end of the twenty-first century (2081–2100) to the beginning of the twenty-first century (2021–40) instead of the historical period (1981–2000).

d. *Land–atmosphere coupling measures*

1) GLACE-1 SUBSEASONAL COUPLING MEASURE $\Delta\Omega$

The GLACE-1 coupling measure Ω_X was defined by Koster et al. (2002, 2004, 2006) as "the degree to which all prescribed boundary conditions affect some atmospheric quantity X" and was estimated for both ensembles using

$$\Omega_X = \frac{16\sigma_{\dot{X}}^2 - \sigma_X^2}{15\sigma_X^2}, \tag{1}$$

with σ_X^2 being the intraensemble variance of X and $\sigma_{\dot{X}}^2$ being the corresponding variance of the ensemble mean time series. In GLACE-1, this measure quantifies subseasonal soil moisture–atmosphere coupling, that is, for ensemble simulations with 16 members that are run over a season only (here JJA or DJF). First, six-day means or totals (means for temperatures, totals for precipitation) are calculated from every simulation. Since the first 8 (JJA) or 6 (DJF, note 7 in leap years) days are disregarded, this leads to 14 six-day means or totals per simulation. The variable σ_X^2 is calculated as the variance across the 224 six-day means or totals from

the whole ensemble. Next, we calculate the ensemble mean time series that is then used to obtain $\sigma^2_{\bar{X}}$ as the variance of the ensemble mean (Koster et al. 2006). The variable $\Delta\Omega_X$ can then be calculated based on the two different variances:

$$\Delta\Omega_X = \Omega_X(R) - \Omega_X(W). \quad (2)$$

We calculate the coupling strength for temperature T and precipitation P.

2) GLACE-CMIP5 COUPLING MEASURE $\Delta\Omega_{\mathrm{GCCMIP5}}$

Seneviratne et al. (2006) proposed alternative Ω and coupling measures to the GLACE-1 Ω and $\Delta\Omega$ to assess the impact of soil moisture–climate coupling on longer time scales ($\Omega_{X,\mathrm{GCCMIP5}}$ and $\Delta\Omega_{X,\mathrm{GCCMIP5}}$). These measures are computed in analogy to the GLACE-1 measures using multiyear simulations instead of ensemble simulations for a single year (or season), with one simulation being fully interactive and the other simulation using prescribed climatological soil moisture (i.e., removing the interannual variability of soil moisture). The variable $\Omega_{X,\mathrm{GCCMIP5}}$ assesses the degree of interannual and intraseasonal similarity in each experiment (Seneviratne et al. 2006):

$$\Omega_{X,\mathrm{GCCMIP5}} = \frac{N\sigma^2_{\bar{X}} - \sigma^2_X}{(N-1)\sigma^2_X}, \quad (3)$$

with N being the number of years $\Omega_{X,\mathrm{IAV}}$ is calculated across (20-yr time periods here). The variable $\sigma^2_{\bar{X}}$ is the variance calculated from the 20-yr climatology, analogous to $\Delta\Omega$, where it is calculated from the ensemble mean. The variable σ^2_X is calculated from 20×14 six-day means. Hence, σ^2_X includes both the interannual as well as the intraseasonal variability. The difference between $\Omega_{X,\mathrm{GCCMIP5}}$ from the control run and from the uncoupled experiment with the prescribed climatological seasonal soil moisture cycle gives the coupling measure $\Delta\Omega_{X,\mathrm{GCCMIP5}}$. Hence, as noted by Seneviratne et al. (2006), $\Omega_{X,\mathrm{GCCMIP5}}$ represents the extent to which the removal of interannual variability of soil moisture increases intraseasonal and interannual similarity (or decreases variability). In these multiyear simulations, $\Omega_{X,\mathrm{GCCMIP5}}$ can be calculated for different time periods. We apply this measure to the GLACE-CMIP5 simulations, using the control run as the coupled simulations and the two experiments A and B as the uncoupled simulations. We use the time periods 1981–2000 (end of twentieth century), 2021–40 (beginning of twenty-first century), and 2081–2100 (end of twenty-first century) to investigate changes in this measure over time.

3) VARIANCE ANALYSIS

We extend the variance analysis defined in Seneviratne et al. (2006) for JJA mean summer temperatures to the Southern Hemisphere summer DJF. It describes the percentage of interannual variance of the mean seasonal temperatures that can be explained by land–atmosphere coupling:

$$\mathrm{VAR} = \frac{\sigma^2_{T(\mathrm{CTL})} - \sigma^2_{T(\mathrm{UNCOUPLED})}}{\sigma^2_{T(\mathrm{CTL})}}. \quad (4)$$

In contrast to $\Delta\Omega_{X,\mathrm{GCCMIP5}}$, this measure only includes interannual variability.

4) CORRELATION BETWEEN EVAPOTRANSPIRATION AND TEMPERATURE

The correlation between evapotranspiration and temperature [correlation(ET, T)] was defined in Seneviratne et al. (2006) for experiments where no GLACE-type simulations were available. It is calculated as the correlation between mean seasonal temperature and mean seasonal evapotranspiration [only JJA in Seneviratne et al. (2006)] for different time periods (here 1981–2000, 2021–40, and 2081–2100). Seneviratne et al. (2006) note that this measure is only meaningful in regions where evapotranspiration is reasonably large. It has the advantage that no special experiments are necessary. Seneviratne et al. (2006) found that it agreed well with the variance analysis and the $\Delta\Omega_{X,\mathrm{GCCMIP5}}$ coupling measure for Europe.

5) SOIL MOISTURE–TEMPERATURE COUPLING MEASURE Π

Miralles et al. (2012) defined an observationally based soil moisture–temperature coupling measure Π based on long-term correlations as

$$\Pi = \rho(H, T) - \rho(H_p, T), \quad (5)$$

where ρ is the Pearson's correlation coefficient, H is an estimate of the sensible heat flux such that $H = R_n - \mathrm{LE}$, and H_p is similar to H but calculated using an estimate of the potential latent heat flux such that $H_p = R_n - \mathrm{LE}_p$. The net radiation R_n and latent heat flux LE can be calculated from the model output. The potential latent heat flux LE_p can be estimated following Priestley and Taylor (1972). As the correlation between temperature and evapotranspiration, Π can be calculated from "normal" model runs or from observational data.

6) TWO-LEGGED COUPLING MEASURE $I_{\mathrm{SM}-T}$

The two-legged index has been used in Dirmeyer (2011) and Dirmeyer et al. (2013a,b, 2014). The terrestrial

first leg can be the influence from any land surface variable on any surface flux (e.g., Dirmeyer 2011). Dirmeyer et al. (2014) presented results for the full index, the influence from soil moisture on sensible heat flux, and the influence of the sensible heat flux on the lifting condensation level. The two-legged index also used correlations between two variables but adds the standard deviation. This accounts for the possibility of a high correlation between two variables coincident with low variability. The first leg, from a land surface variable A to a surface flux B, is

$$I_{A-B} = \sigma(B)\rho(A,B) = \sigma(A)\frac{dB}{dA}. \quad (6)$$

The full two-legged index is then derived by adding the second leg from the surface flux B to the atmospheric variable C:

$$I_{A-C} = \sigma(C)\rho(A,B)\rho(B,C) = \sigma(A)\frac{dB}{dA}\frac{dC}{dB}. \quad (7)$$

We use soil moisture as the land surface variable (A), the sensible heat flux (B), and near-surface air temperature as the atmospheric variable (C) to be able to compare this two-legged measure to the other measures.

7) QUANTILE REGRESSION ANALYSIS

The quantile regression analysis relates the number of hot days and the 3-month standard precipitation index (SPI3) in the preceding month at each grid point. The SPI3 acts as a proxy for soil moisture. The highest quantile, 90th is most representative for an extremely high number of hot days. This analysis can be derived from temperature and precipitation data only, and this or very similar methods have been widely used to approximate soil moisture–temperature coupling from observational data (Hirschi et al. 2011; Mueller and Seneviratne 2012; Ford and Quiring 2014). We define the number of hot days by the number of days where the maximum daily temperature is above the 90th percentile during 1961–90 (TX90p; Zhang et al. 2011). The more negative the slope of the 90th quantile regression, the higher the influence from low SPI3 on a high number of hot days. We only include this measure for the present-day analysis because it would need to be adjusted for future projections (by revising the reference 90th percentile and the reference period for SPI3). We also include this measure because it only requires temperature and precipitation and is therefore particularly useful when comparing to observational data and when future simulation data are limited. We calculate the SPI and quantile regression using R (packages SCI and quantreg).

TABLE 1. Thresholds for measures to be considered as coupled in Figs. 12 and 13. The averages were used for 2081–2100.

Measure	DJF	JJA	Average
Strongly coupled			
$\Delta\Omega$ GLACE-1	0.1	0.1	—
$\Delta\Omega$ GLACE-CMIP5	0.1096	0.0887	0.10
Variance	28.692	26.0987	27
Correlation(ET, T)	−0.4428	−0.3466	−0.39
Π	0.3099	0.4899	0.40
I_{SM-T}	−0.2639	−0.2201	−0.24
90th quantile slope	−2.0241	−2.0600	−2.04
Very strongly coupled			
$\Delta\Omega$ GLACE-1	0.2	0.2	—
$\Delta\Omega$ GLACE-CMIP5	0.1467	0.1387	0.14
Variance	41.3489	38.4714	40
Correlation(ET, T)	−0.5988	−0.6189	−0.61
Π	0.6025	0.9858	0.79
I_{SM-T}	−0.4844	−0.5474	−0.52
90th quantile slope	−2.6696	−3.0463	−2.86

e. *Agreement between land–atmosphere coupling measures*

To investigate the agreement between the different coupling measures, we scaled the different measures to account for their different numeric ranges. The coupling measures defined by $\Delta\Omega$ and Π lie mainly between 0 and 1. The variance analysis results in values between 0% and 100%. The correlation(ET, T) lies in between −1 and 1. The I_{SM-T} leads to values in the range from around −2 to 0.5. The quantile regression slopes can be anything from $-\infty$ to ∞, but we are interested in the regions where the slope is negative. Further, a value of 1 for $\Delta\Omega$ does not correspond to 100% in the variance analysis. In short, it is not clear which value in one measure corresponds to another value in another measure. We therefore define the average of $\Delta\Omega_T$ from the three GLACE-1 experiments as a reference. We then use the model range from Koster et al. (2006) to examine the spatial and seasonal distribution of values above 0.1 for strongly coupled and 0.2 for very strongly coupled regions. We scale the other measures to cover the same land area for the thresholds we define as "strongly coupled" and "very strongly coupled." The resulting thresholds are provided in Table 1.

3. Results

a. *GLACE-1 results from ACCESS1.3b*

The ACCESS1.3b model is among the more strongly coupled models for temperature. Koster et al. (2006, their Fig. 8) showed the global distribution of $\Delta\Omega_T$ for 1994, which can be compared with Fig. 2c. ACCESS1.3b shows similar patterns of strong and weak

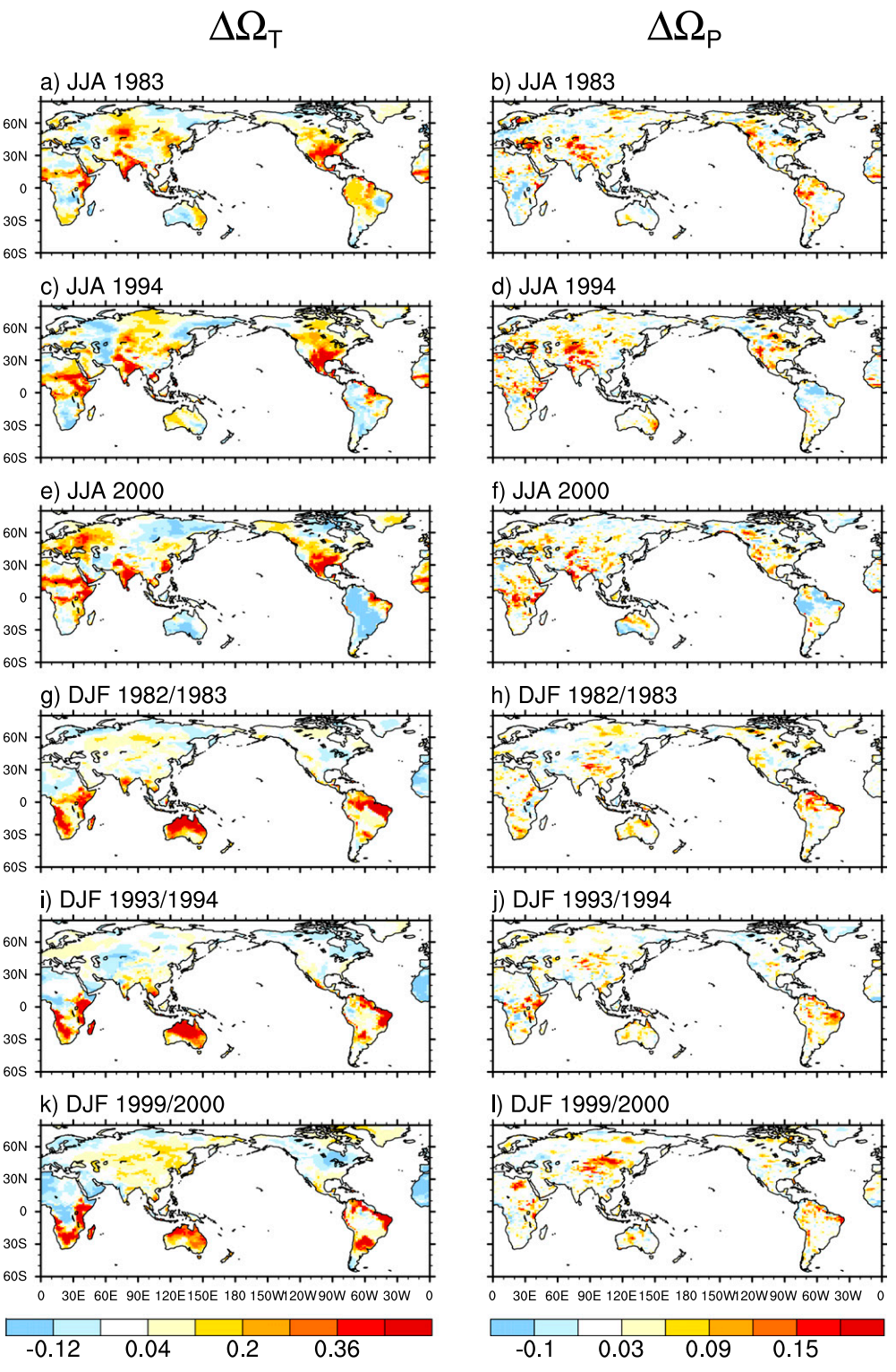

FIG. 2. GLACE-1 coupling strength $\Omega_X(R) - \Omega_X(W)$ in (a),(b) JJA 1983; (c),(d) JJA 1994; (e),(f) JJA 2000; (g),(h) DJF 1982/83; (i),(j) 1993/94; and (k),(l) 1999/2000 for (left) mean temperature and (right) total precipitation. The content of (c) corresponds to Fig. 8 of Koster et al. (2006) for JJA mean temperature and of (d) corresponds to Fig. 5 of Koster et al. (2006) for JJA total precipitation.

soil moisture–temperature coupling for the boreal summer in comparison to GFDL, CCCma, and the CSIRO Conformal Cubic version 3 (CSIRO-CC3) models with particularly strong coupling over central Africa, central Eurasia, and North America. Similar to other GLACE-1 models, ACCESS1.3b is relatively weakly coupled over eastern Eurasia and parts of western Europe. In short, soil moisture–temperature coupling strength of ACCESS1.3b for JJA 1994 is within the range reported by Koster et al. (2006) for 1994, even though there was a small difference in the experiment setup by prescribing all soil layers. The locations of strong $\Delta\Omega_T$ vary between years. Using 1983 conditions (Fig. 2a, El Niño year) the differences from 1994 (Fig. 2c, neutral year) are very small in the Northern Hemisphere and are negligible compared to the intermodel range in $\Delta\Omega_T$ reported by Koster et al. (2006). A major difference occurs over eastern Europe for 2000 (Fig. 2e, La Niña), with the weak coupling (1983 and 1994) being replaced by a strong coupling. A second major difference occurs over South America, which is strongly coupled in 1983 (Fig. 2a) and weakly coupled in 2000 (Fig. 2e). Broadly, however, the ranges in $\Delta\Omega_T$ simulated by ACCESS1.3b for JJA are more similar across the 3 years examined than among the 12 models examined by Koster et al. (2006).

Results from ACCESS1.3b suggest very strong Southern Hemisphere soil moisture–temperature coupling during DJF in southern Africa, Australia, and those regions in South America not covered by tropical forest. The values of $\Delta\Omega_T$ for DJF (Figs. 2g,i,k) are higher than those found for JJA by Koster et al. (2006), noting that austral summer (DJF) results for $\Delta\Omega_T$ were not reported by Koster et al. (2006). Regions where $\Delta\Omega_T$ is large are broadly consistent across the 3 years we examined, although Australia shows some variability in coupling strength between the years.

Soil moisture–precipitation coupling in ACCESS1.3b (Figs. 2b,d,f) for JJA is also within the range of the models shown in Koster et al. (2006, their Fig. 5). In contrast to soil moisture–temperature coupling, where ACCESS1.3b was among the more strongly coupled models, the model is among the more weakly coupled for $\Delta\Omega_P$. Note that the range of soil moisture–precipitation coupling strength is smaller than for soil moisture–temperature coupling strength (Koster et al. 2006). Large values of $\Delta\Omega_P$ do occur in some regions, including parts of North America, north of India, and central Africa, and these areas appear to be relatively strongly coupled in all years examined. In DJF, the soil moisture–precipitation coupling is weaker, although parts of South America, tropical Africa, and Asia are relatively strongly coupled (Figs. 2h,j,l). The differences in $\Delta\Omega_P$ among the three time periods examined are small relative to the range highlighted by Koster et al. (2006). The strength of the coupling of $\Delta\Omega_P$ is consistently weaker in ACCESS1.3b compared with the models examined by Koster et al. (2006).

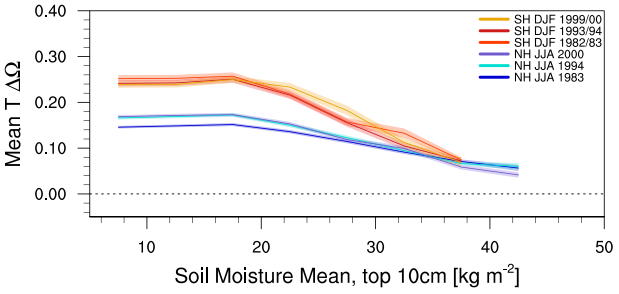

FIG. 3. GLACE-1 coupling strength $\Delta\Omega_T$ vs mean soil moisture ($kg\,m^{-2}$) for all years. Northern Hemisphere data are averaged over 0°–60°N for JJA and Southern Hemisphere data are averaged over 60°S–0° for DJF.

We can also examine the coupling strength for $\Delta\Omega_T$ versus mean soil moisture for all years averaged over the two hemispheres (Fig. 3). For both hemispheres, the coupling strengths decline at soil moistures above $20\,kg\,m^{-2}$. The variable $\Delta\Omega_T$ is much higher for low values of soil moisture in the Southern Hemisphere summer (red lines in Fig. 3) compared to the Northern Hemisphere summer (blue lines in Fig. 3). At high soil moisture values, the Southern Hemisphere values decline to be the same as in the Northern Hemisphere. Hence, there is a much larger range of coupling strengths and a stronger relationship between $\Delta\Omega_T$ and soil moisture in the Southern Hemisphere summer.

b. GLACE-CMIP5 with ACCESS1.3b

1) $\Delta\Omega_{T,\mathrm{GCCMIP5}}$ COUPLING STRENGTH

The coupling strengths for the GLACE-CMIP5 experiments were calculated for the end of the twentieth century (1981–2000), the beginning of the twenty-first century (2021–40), and the end of the twenty-first century (2081–2100). The coupling strength obtained from these multiyear experiments indicates the extent to which the removal of both the interannual variability and trend (ExpA) or the removal of only the interannual variability (ExpB) in soil moisture affects the similarity. A large increase in similarity in the experiments is associated with strong coupling.

For the DJF 1981–2000 mean temperature (Fig. 4a), ACCESS1.3b shows strong coupling over large regions of North America and Australia for ExpA. There is a stronger and more widespread impact in the experiments

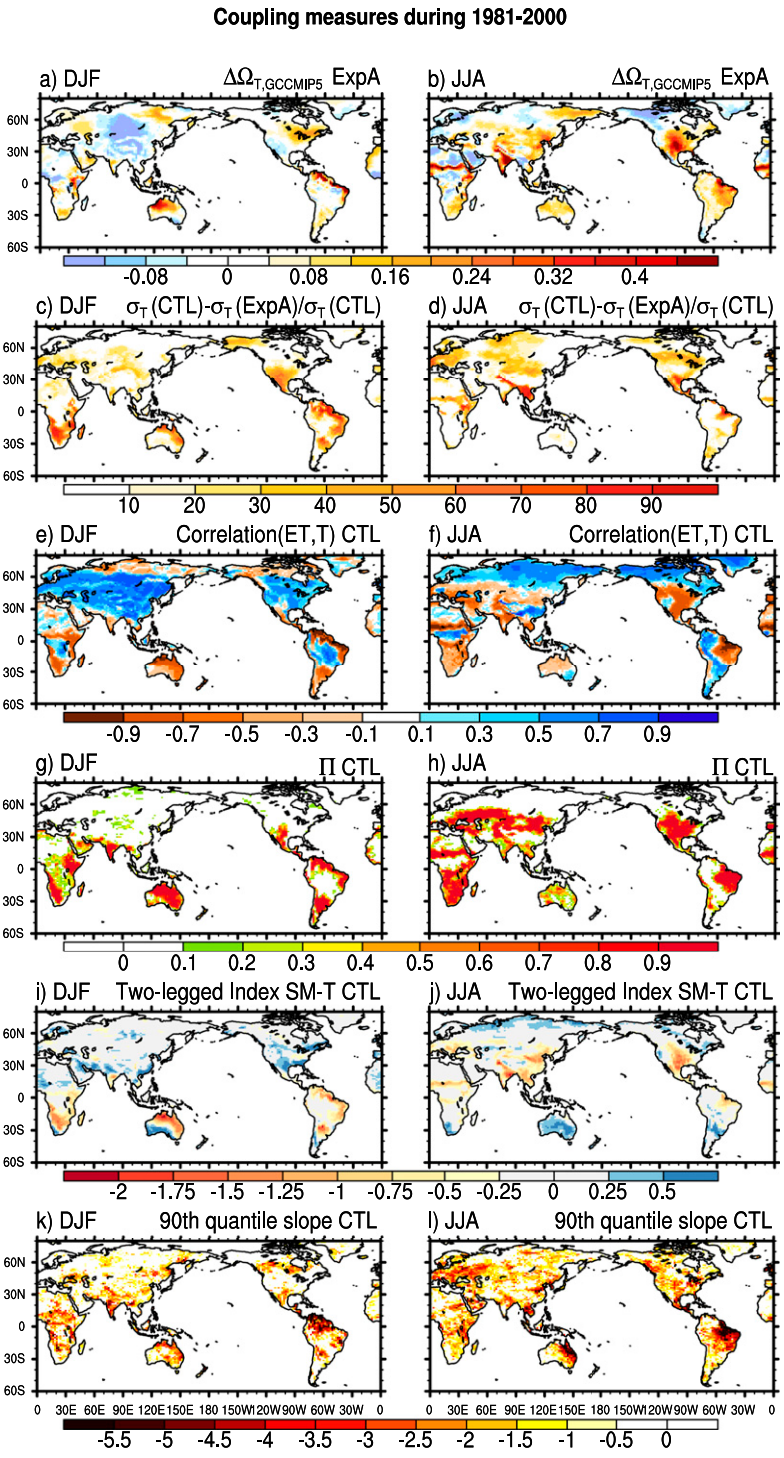

FIG. 4. Soil moisture–temperature coupling measures for 1981–2000 during (left) DJF and (right) JJA: (a),(b) the $\Delta\Omega_{T,GCCMIP5}$ coupling strength for ExpA [this corresponds to Fig. 2c in Seneviratne et al. (2006) for JJA]; (c),(d) the variance analysis for ExpA [this corresponds to Fig. 2a in Seneviratne et al. (2006) for JJA]; (e),(f) the correlation(ET, *T*) for CTL [this corresponds to Figs. 3a,d,g in Seneviratne et al. (2006) for JJA]; (g),(h) the soil moisture–temperature coupling metric for CTL [this is comparable with Fig. 1 in Miralles et al. (2012)]; (i),(j) the two-legged soil moisture–temperature coupling index for CTL; and (k),(l) the slope of 90th quantile regression analysis for the number of hot days and the preceding SPI in CTL [this is comparable with Fig. 3d in Mueller and Seneviratne (2012)].

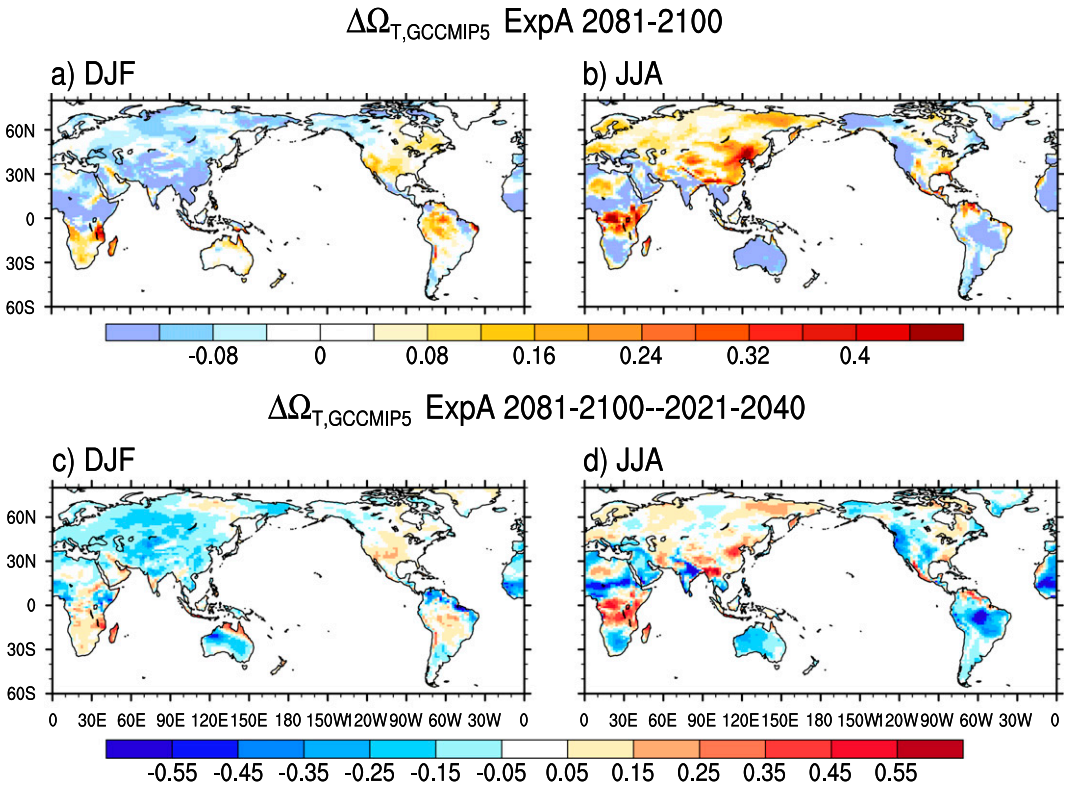

FIG. 5. (a),(b) The $\Delta\Omega_{T,\mathrm{GCCMIP5}}$ coupling strength for temperature at the end of the twenty-first century and (c),(d) the difference in the $\Delta\Omega_{T,\mathrm{GCCMIP5}}$ coupling strength between the end and beginning of the twenty-first century (2081–2100 minus 2021–40) for ExpA during (left) DJF and (right) JJA.

in JJA with a strong coupling over large regions of Eurasia, southern Africa, Australia, and North and South America. These results, for ExpA, point to increases in similarity for temperature in some areas of the globe if both interannual variability and the trend in soil moisture are removed. These areas correspond largely to the areas shown as strongly coupled in the GLACE-1 experiments. Results for ExpB (not shown) are almost identical to ExpA at the end of the twentieth century because there is no consistent trend in soil moisture over this period (see Fig. 1).

2) VARIANCE ANALYSIS

The variance analysis (section 2d) examines the difference in variance in temperature between the control simulation and ExpA normalized by the variance in the control simulation. Figures 4c and 4d show the variance analysis at the end of the twentieth century and highlight regions of high influence of land–atmosphere coupling on variance, particularly in the summer hemisphere. For the Southern Hemisphere in DJF (Fig. 4c) regions including South America, southern Africa, and northern Australia show high percentages, implying that land–atmosphere coupling plays a significant role. In JJA (Fig. 4d) parts of North America, western Europe, and Eurasia also display high percentages from the variance analysis.

Most regions where there is a high percentage (>50%) of interannual variance explained by land–atmosphere coupling (Figs. 4c,d) are also strongly coupled according to $\Delta\Omega_{T,\mathrm{GCCMIP5}}$ (Figs. 4a,b). One region that did not show strong coupling based on $\Delta\Omega_{T,\mathrm{GCCMIP5}}$ but has more than 90% of its temperature variance explained by land–atmosphere coupling is Southeast Asia in JJA. Western Europe in JJA also has around 50% of its temperature variance explained by land–atmosphere coupling, even though it did not show strong coupling in Fig. 4b.

Overall, the percentage of temperature variance explained by land–atmosphere coupling estimated in Figs. 4c and 4d provides a broadly similar, but regionally very different picture than $\Delta\Omega_{T,\mathrm{GCCMIP5}}$. The two measures examine slightly different aspects of the influence of soil moisture. The variable $\Delta\Omega_{T,\mathrm{GCCMIP5}}$ estimates the extent to which the removal of soil moisture variability increases interannual and intraseasonal similarity, whereas the variance analysis estimates the percentage of interannual variance explained by land–atmosphere

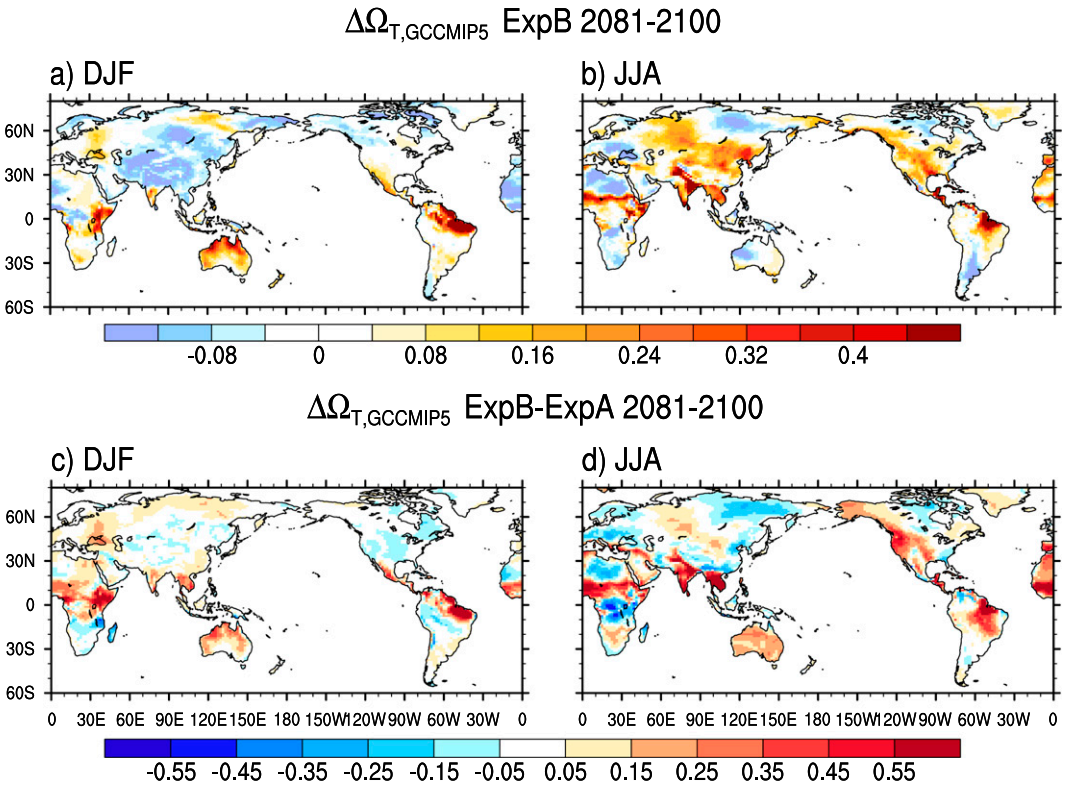

FIG. 6. (a),(b) The $\Delta\Omega_{T,\mathrm{GCCMIP5}}$ coupling strength for temperature at the end of the twenty-first century in ExpB and (c),(d) the difference in the $\Delta\Omega_{T,\mathrm{GCCMIP5}}$ coupling strength between ExpB and ExpA for the end of twenty-first century (2081–2100) during (left) DJF and (right) JJA.

coupling. This difference in definition leads to different results in some areas of the globe.

3) CORRELATION BETWEEN TEMPERATURE AND EVAPOTRANSPIRATION

Another measure to estimate land–atmosphere coupling, used by Seneviratne et al. (2006), is the correlation between temperature and evapotranspiration (section 2d). Here, we compare this measure to the $\Delta\Omega_{T,\mathrm{GCCMIP5}}$ coupling strength and the variance analysis with the aim of determining whether this measure leads to conclusions consistent with other coupling strength measures.

Most regions showing a large negative correlation between temperature and evapotranspiration (Figs. 4e,f) agree well with strongly coupled regions shown in Figs. 4a and 4b. However, the regions showing negative correlations are larger than those with strong coupling defined by $\Delta\Omega_{T,\mathrm{GCCMIP5}}$. As discussed by Seneviratne et al. (2006), the correlation between temperature and evapotranspiration is only a good measure for land–atmosphere coupling if evapotranspiration is reasonable large; hence, regions where this is not the case need to be excluded (e.g., Middle East in JJA).

4) SOIL MOISTURE–TEMPERATURE COUPLING MEASURE

The soil moisture–temperature coupling measure highlights similar regions to the other measures. In DJF (Fig. 4g), strong coupling is mainly constrained to the Southern Hemisphere, excluding regions covered by rain forest. India and southwestern North America are the only Northern Hemisphere regions that are indicated to be influenced by land–atmosphere interactions in DJF. In JJA (Fig. 4h) large regions in North America, Eurasia, eastern South America, and Southern Africa show high values of this measure. These regions are considerably larger than shown in Figs. 4a and 4b but compare very well to the correlation of temperature and evapotranspiration in Figs. 4e and 4f.

5) TWO-LEGGED SOIL MOISTURE–TEMPERATURE COUPLING INDEX

The two-legged soil moisture–temperature coupling index ($I_{\mathrm{SM}-T}$) highlights similar regions as the other coupling measures (Figs. 4i and 4j); however, the strongly coupled regions are relatively small. This indicates that this index is rather restrictive in its definition

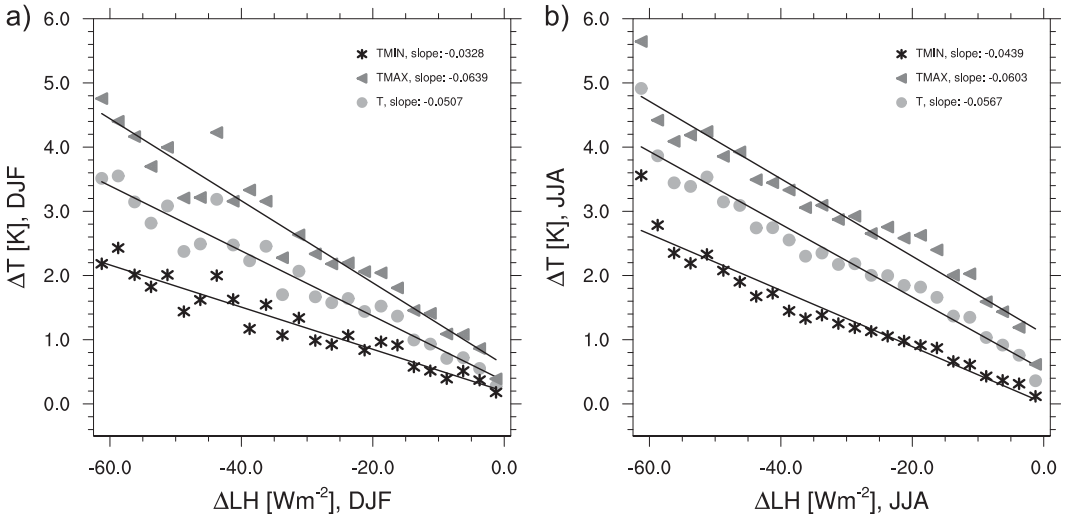

FIG. 7. Scatterplot and linear regression of ΔT, ΔT_{MAX}, and ΔT_{MIN} vs ΔLH [K $(\mathrm{W\,m^{-2}})^{-1}$] in simulations ExpB minus ExpA at the end of the twenty-first century (2081–2100) for (a) DJF over the Southern Hemisphere (60°S–0°) and (b) JJA over the Northern Hemisphere (0°–60°N). Analyses only include land points and areas with negative ΔLH, using bins of 2.5 $\mathrm{W\,m^{-2}}$ for ΔLH. This corresponds to Fig. 4a in Seneviratne et al. (2013).

for strongly coupled regions, probably because it includes the two pathways, from soil moisture to the surface flux and then from the surface flux to temperature.

6) 90TH QUANTILE REGRESSION SLOPE BETWEEN HOT DAYS AND PRECEDING SPI

In the figure for the 90th quantile slopes (Figs. 4k,l), negative slopes indicate that with drier conditions (negative value of SPI) there are a larger number of hot days. The most pronounced slopes of the 90th quantile regression are generally collocated with strong land–atmosphere coupling identified from other measures. An exception is northeastern Australia, which shows a strongly negative slope in JJA but no strong coupling in other measures. In addition, the area of strongly negative slopes in Amazonia is larger than indicated by the other measures. There is also a rather strong negative slope in eastern Europe in JJA that is not present in all the other measures. North America in JJA, on the other hand, shows smaller negative slopes than indicated from other measures. The very strong negative slopes in northeastern Brazil in DJF are also suggested by the other measures, even if the area of strongly negative slopes is larger than in most other measures.

7) FUTURE PROJECTIONS OF LAND–ATMOSPHERE COUPLING

We next examine ACCESS's coupling strength under future climate conditions. Figure 5 shows the coupling strength for ExpA at the end of the twenty-first century (Figs. 5a,b) and the difference in $\Delta\Omega_{T,\mathrm{GCCMIP5}}$ coupling strength between the end and the beginning of the twenty-first century for ExpA in ACCESS1.3b for T (Figs. 5c,d). The most obvious change in coupling strength from ExpA is that most strongly coupled regions show a decrease in $\Delta\Omega_{T,\mathrm{GCCMIP5}}$ toward the end of the twenty-first century. Several regions show an increase in coupling strength into the future. Figure 6 shows the $\Delta\Omega_{T,\mathrm{GCCMIP5}}$ coupling strength for ExpB and the difference between ExpB and ExpA at the end of the twenty-first century. The coupling strength tends to be higher in ExpB compared to ExpA. This indicates that a large portion of the decrease in coupling strength in ExpA between the beginning and end of the twenty-first century is associated with the omitted trend in soil moisture. The $\Delta\Omega_{T,\mathrm{GCCMIP5}}$ coupling strength in ExpB at the end of the twenty-first century (Figs. 6a,b) is similar to the one found for the end of the twentieth century (Figs. 4a,b) but increased and expanded, especially in the Southern Hemisphere in DJF.

The differences between temperatures and latent heat fluxes in experiments A and B at the end of the twenty-first century show a linear relationship where the latent heat flux is smaller in ExpB compared to ExpA in ACCESS1.3b (Fig. 7). The slope of this curve is steepest for maximum temperature T_{MAX} and flattest for minimum temperature T_{MIN}, with T in the middle for both hemisphere summers. A very similar relationship was shown by Seneviratne et al. (2013) for the GLACE-CMIP5 ensemble mean (their Fig. 4a) for the Northern Hemisphere summer. The gradient of these curves is slightly smaller in the Southern Hemisphere DJF (Fig. 7a)

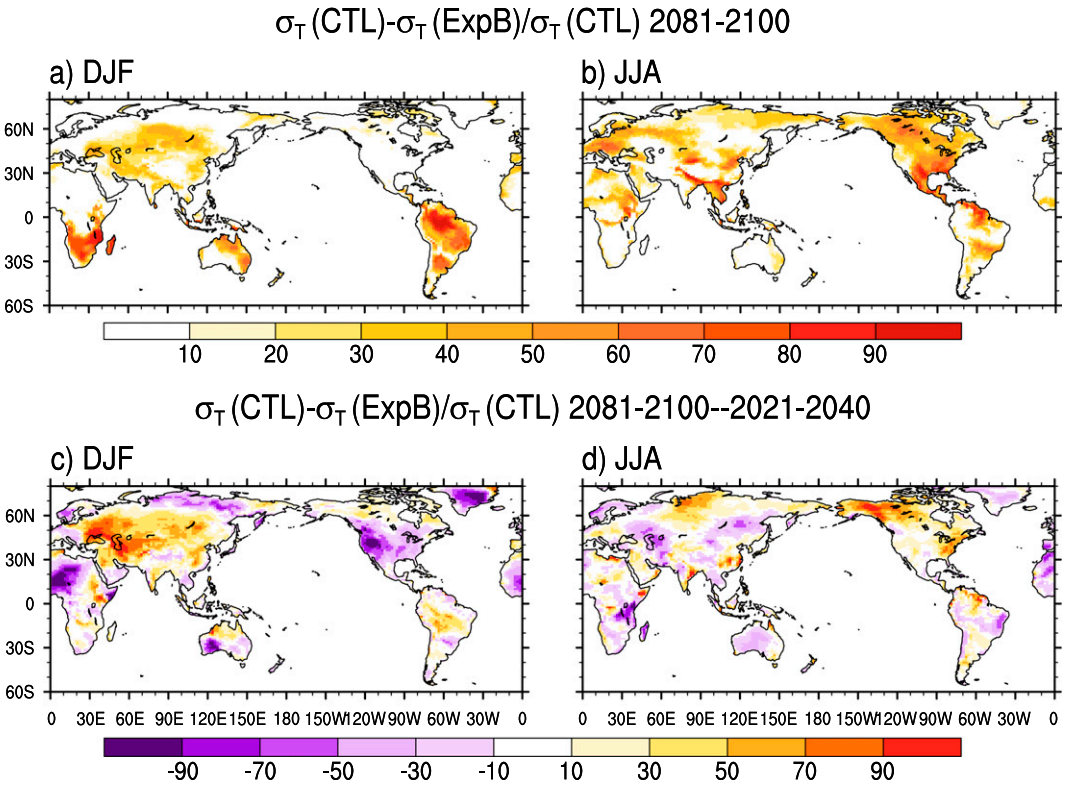

FIG. 8. (a),(b) The variance analysis for temperature for the end of the twenty-first century (2081–2100) in ExpB and (c),(d) the difference between the end and beginning of the twenty-first century (2081–2100 minus 2021–40) during (left) DJF and (right) JJA. Except for the included soil moisture trend in ExpB, (b) corresponds with Fig. 2b in Seneviratne et al. (2006).

compared to Northern Hemisphere JJA (Fig. 7b) for T_{MIN} and T and very similar for T_{MAX}. This implies that in areas where the soil moisture trend in ExpB leads to a decrease in latent heat flux, temperatures are linearly increased. This relationship is strongest for T_{MAX} and weakest for T_{MIN} and is similar in both hemispheres.

Figures 8a and 8b show the variance analysis at the end of the twenty-first century. Since the relevance of the soil moisture trend is limited to the future runs (see Fig. 6 and section 4), we calculate the variance analysis for ExpB. The broad patterns for the variance analysis (Figs. 4c,d) change through to the end of the twenty-first century (Figs. 8c,d). For example, the variance measure increases over North America, parts of Amazonia, and Siberia in JJA and eastern Europe, Asia, northern Australia, and Amazonia in DJF, implying that land–atmosphere coupling plays an increasing role in explaining temperature variance. In contrast, the percentage of temperature variance that can be explained by land–atmosphere coupling decreases over North America, North Africa, and southwestern Australia in DJF. These changes do not correspond to the changes seen in $\Delta\Omega_{T,GCCMIP5}$ (Figs. 5c,d and 6c,d).

The future pattern (2081–2100) in the temporal correlation of ET and T (Figs. 9a,b) can be compared to Figs. 4e and 4f for 1981–2000. The present and future patterns are similar, with a similar seasonal variability and intensity of coupling strength. There are small changes in correlation(ET, T) from 2081–2100 to 2021–40 (Figs. 9c,d). The correlation(ET, T) becomes increasingly negative with time over regions of Eurasia in JJA and over North America in DJF and JJA. The largest change occurs over Amazonia in DJF, where the region with negative correlation is expanded.

The soil moisture–temperature coupling measure Π shows a very similar pattern at the end of the twenty-first century (Figs. 10a,b) compared to the twentieth century (Figs. 4g,h). Some of the coupling regions are increased (Amazonia in DJF and North America and Europe in JJA). Eastern Australia in JJA emerges as a new region with an indication for strong influence from the land surface on temperature, although Π is the only measure showing this.

The two-legged index (Fig. 11) shows increases in land–atmosphere coupling in central and southern Africa, India, and Amazonia in DJF and over large parts of

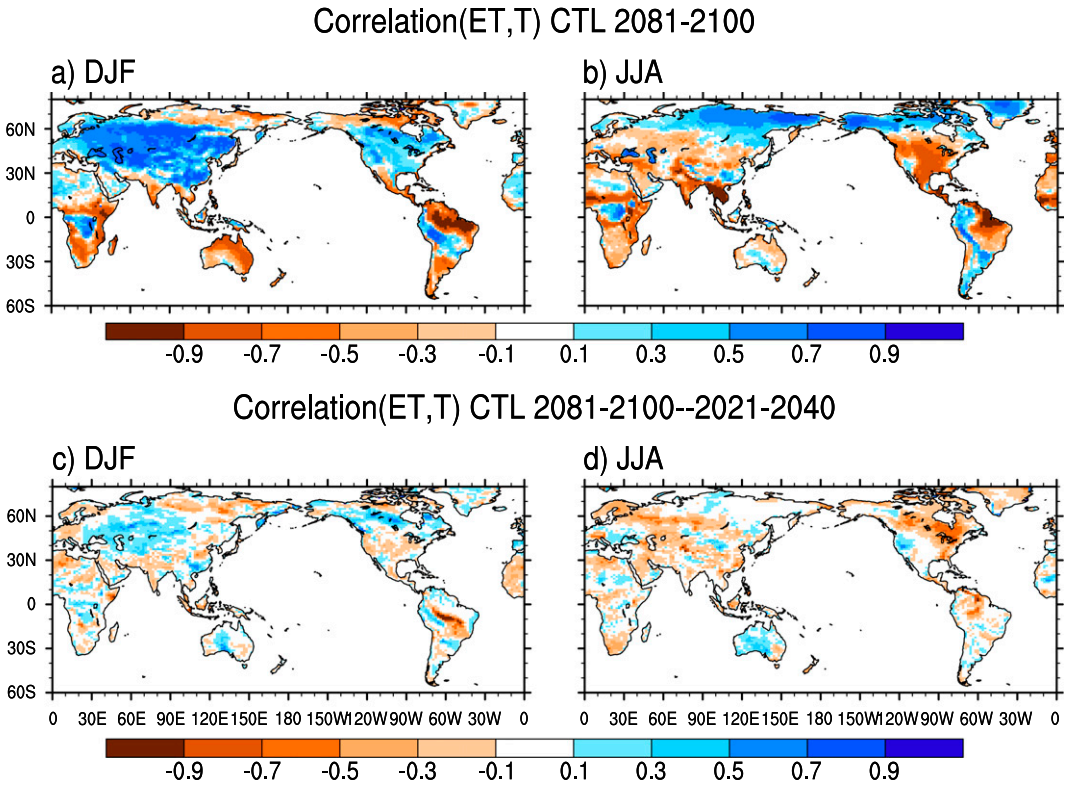

FIG. 9. (a),(b) The correlation(ET, *T*) for the CTL at the end of the twenty-first century (2081–2100) and (c),(d) the difference between the end and beginning of the twenty-first century (2081–2100 minus 2021–40) during (left) DJF and (right) JJA. The content in (b) corresponds to Figs. 3b, 3e, and 3h in Seneviratne et al. (2006), and in (d) corresponds to Figs. 3c, 3f, and 3l in Seneviratne et al. (2006).

the Northern Hemisphere and the north of South America in JJA from 2021–40 to 2081–2100. The dominating increase in this measure into the future is consistent with Dirmeyer et al. (2013b), who found an increasing trend in land–atmosphere coupling in CMIP5 simulations.

4. Discussion

There are three key results that are worthy of discussion: the differences between the Southern and Northern Hemisphere, the agreement between the different coupling measures, and the changes in land–atmosphere coupling into the future. First, we demonstrated for GLACE-1 that the coupling strength was approximately twice as strong for the Southern Hemisphere compared to the Northern Hemisphere (Figs. 2, 3), particularly for temperature. Most of the Southern Hemisphere land was strongly coupled and fewer areas were weakly coupled. In contrast, the average across the Northern Hemisphere contains large weakly coupled regions. The Northern Hemisphere hot spots occur in transition regions between wet and dry climates, whereas in the Southern Hemisphere we find a strong signal in the tropics and subtropics. Given the lack of previous examination of Southern Hemisphere summer coupling strengths using the GLACE-1 method, it is not possible to explore whether these results are model specific or would be reproduced in other climate models. It would be useful to explore the influence of prescribing the whole soil column in comparison to not prescribing the top soil layer (see Koster et al. 2004, 2006) to see if this explains the hemispheric differences. We did examine the ratio of bare soil evaporation to total evaporation and found it to be slightly higher in Southern Hemisphere summer.

Our second key area of discussion is whether the different measures used to derive a coupling strength lead to similar conclusions. We showed that different coupling measures vary in their level of agreement. There is similarity in the coupling strengths estimated via the two $\Delta\Omega$ methods for GLACE-1 and GLACE-CMIP5, and regions strongly coupled in GLACE-1 (Fig. 2) are broadly similar to those in GLACE-CMIP5 (Figs. 4a,b). Conclusions reached from GLACE-1 would

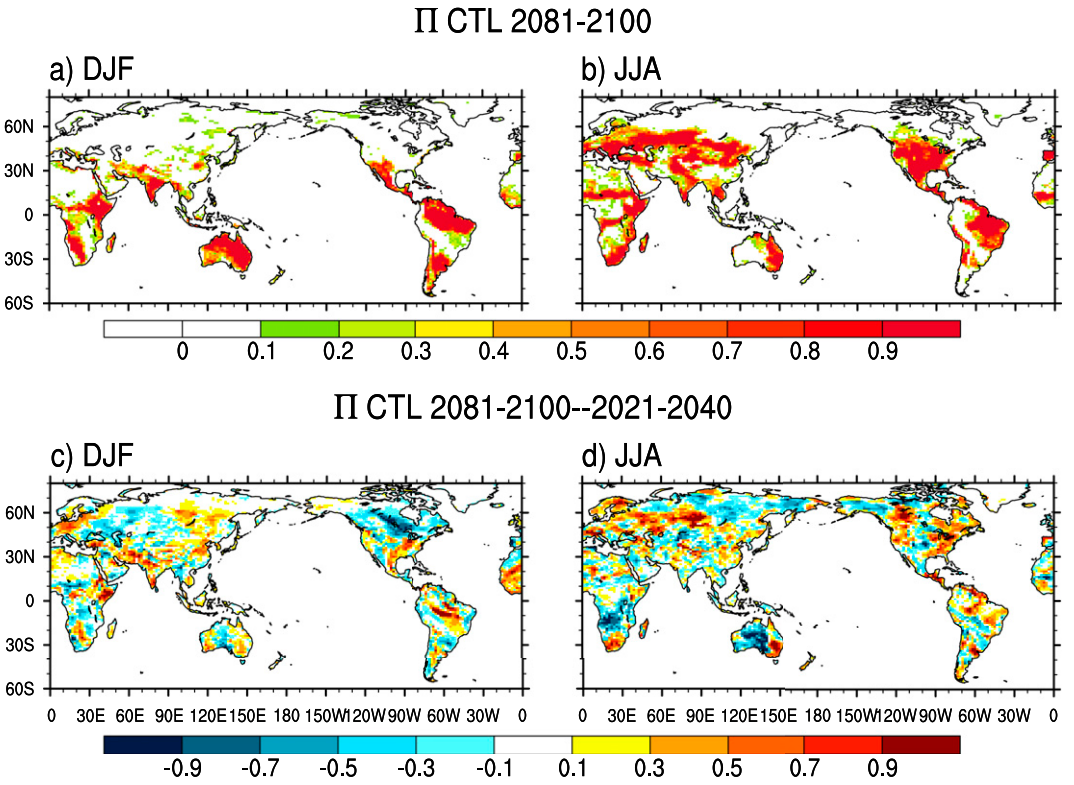

FIG. 10. (a),(b) The soil moisture–temperature coupling metric for CTL at the end of the twenty-first century (2081–2100) and (c),(d) the difference between the end and beginning of the twenty-first century (2081–2100 minus 2021–40) during (left) DJF and (right) JJA.

therefore be matched by those from GLACE-CMIP5 with ACCESS1.3b. The actual numerical values from GLACE-CMIP5 need to be scaled by roughly a factor of 1.5 to give values of a similar magnitude to GLACE-1. We encourage those modeling groups involved in GLACE-CMIP5 to conduct a GLACE-1 experiment to confirm our results.

For ACCESS1.3b, the similarity between the other coupling measures is less well defined. These measures are very different from each other with different ranges of values. The main issue we encountered was how to define a threshold value for $\Delta\Omega_T$, $\Delta\Omega_{T,\mathrm{GCCMIP5}}$, variance analysis, correlation(ET, T), Π, $I_{\mathrm{SM}-T}$, and quantile regression slope that defines a strongly coupled region because the numerical values are not interchangeable. To examine this issue further, we took GLACE-1 $\Delta\Omega_T$ as our baseline definition of strongly coupled and used the model range from Koster et al. (2006) to examine the spatial and seasonal distribution of values above 0.1 for strongly coupled and 0.2 for very strongly coupled regions. We then chose thresholds for the other three measures such that the same percentage of the land surface falls into these categories (see Table 1, Fig. 12). Figure 12 shows the regions where the measures agree on strongly coupled (Figs. 12a,b) and very strongly coupled (Figs. 12c,d) areas. While there is good agreement for the regions we have already identified as coupling hot spots based on the individual measures, all seven measures rarely agree, and many regions that appear strongly coupled in one measure are not identified as strongly coupled in others (see purple regions in Fig. 12). There is also some disagreement on the spatial extent of these regions. Based on the maps showing the single measures (Figs. 2, 4), we identified which coupling measure was giving these apparent false alarms. Unfortunately, all six measures based on the GLACE-CMIP5 runs are responsible for explaining specific false alarms, and no single measure shows considerable more false alarms than the others.

To avoid any misunderstanding, we note that the threshold values shown in Table 1 are ACCESS1.3b specific and cannot be applied to other climate models. Our results highlight that using the more simply derived measures as surrogates for the more computationally expensive GLACE-1 and GLACE-CMIP5 measures needs to be undertaken carefully. We suggest that a model would need to undertake an analysis like the one

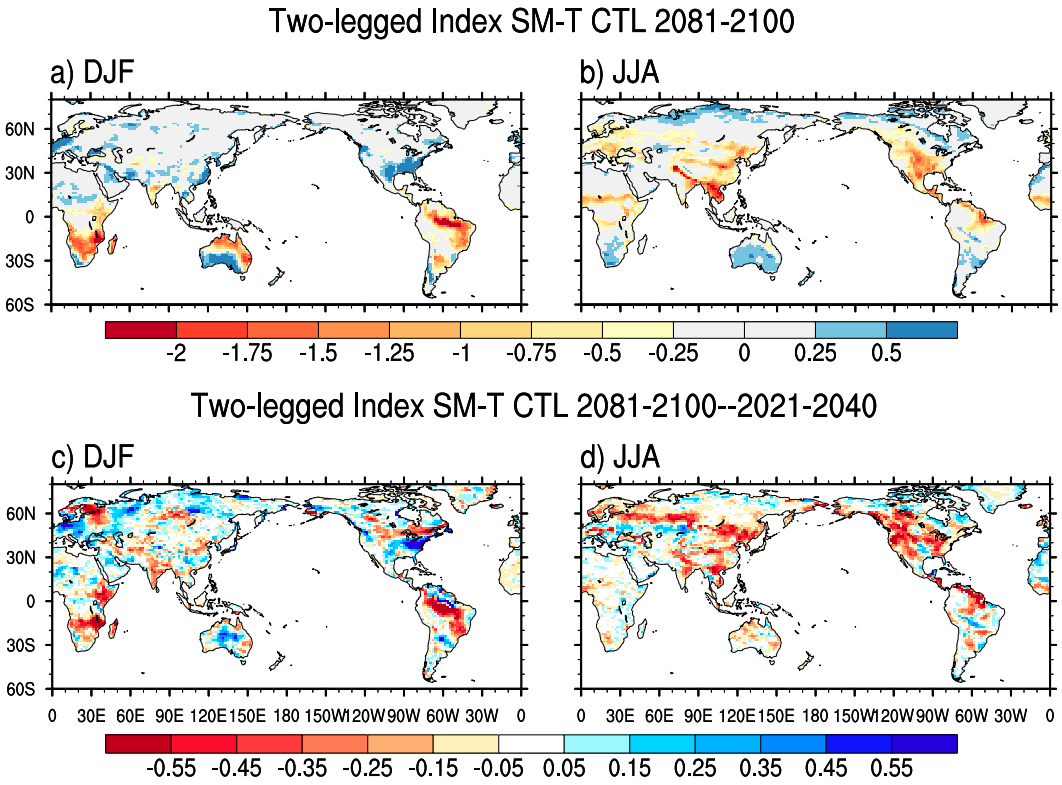

FIG. 11. (a),(b) The two-legged soil moisture–temperature coupling index for CTL at the end of the twenty-first century (2081–2100) and (c),(d) the difference between the end and beginning of the twenty-first century (2081–2100 minus 2021–40) during (left) DJF and (right) JJA. Keep in mind that a negative difference means stronger coupling.

reported here to establish how well the correlation of evapotranspiration and temperature, Π, I_{SM-T}, and especially quantile regression slope reproduced the GLACE-1 and GLACE-CMIP5 before the simpler measures were used in analyses. In particular, it needs to be established what values of correlation(ET, T), Π, I_{SM-T}, and quantile regression slope correspond to strongly coupled regions for each individual model. Once this is known, the correlation(ET, T), Π, and I_{SM-T} lead to the identification of very similar coupling hot spots to those from the GLACE-1 and GLACE-CMIP5 experiments.

Finally, and in agreement with Seneviratne et al. (2013), we find that a possible soil moisture trend is important for the soil moisture–atmosphere coupling at the end of the twenty-first century. Using GLACE-CMIP5 experiments A and B, we are able to distinguish between the influence from soil moisture variability and soil moisture trend on coupling strength. Removing the trend as well as the interannual variability results in a decrease in soil moisture–temperature coupling in large areas over the globe. If we include the soil moisture trend in ExpB, the coupling strength is larger than without it in many areas (Fig. 6). Hence, the soil moisture trend plays a major role in how coupling strength changes in the future and highlights the need to capture a possible trend in future projections. A similar analysis to the one performed for Fig. 12 can be undertaken for the future results from GLACE-CMIP5. We used the thresholds presented in Table 1 and applied them to the five GLACE-CMIP5 measures. It is important to note that only two of the five measures depend on experiments A and B. Figures 13a–d show that there is some agreement for the major coupling hot spots in ExpA. For DJF (Figs. 13a,c), we obtain larger areas where all five measures agree. In JJA (Figs. 13b,d) many areas are identified as strongly coupled by only one measure, and disagreement is rather high outside of the hot spot regions. In ExpB (Figs. 13e–h) the agreement between the measures is larger than in ExpA, and the same regions are identified as coupling hot spots as in present climate conditions. Hot spot areas where five measures agree tend to expand in future projections. Our results suggest that any future drying trend, which is projected by ACCESS, will lead to similar but expanded regions of strong land–atmosphere coupling than for the present climate. If any possible trend is not taken into account, different coupling measures tend to

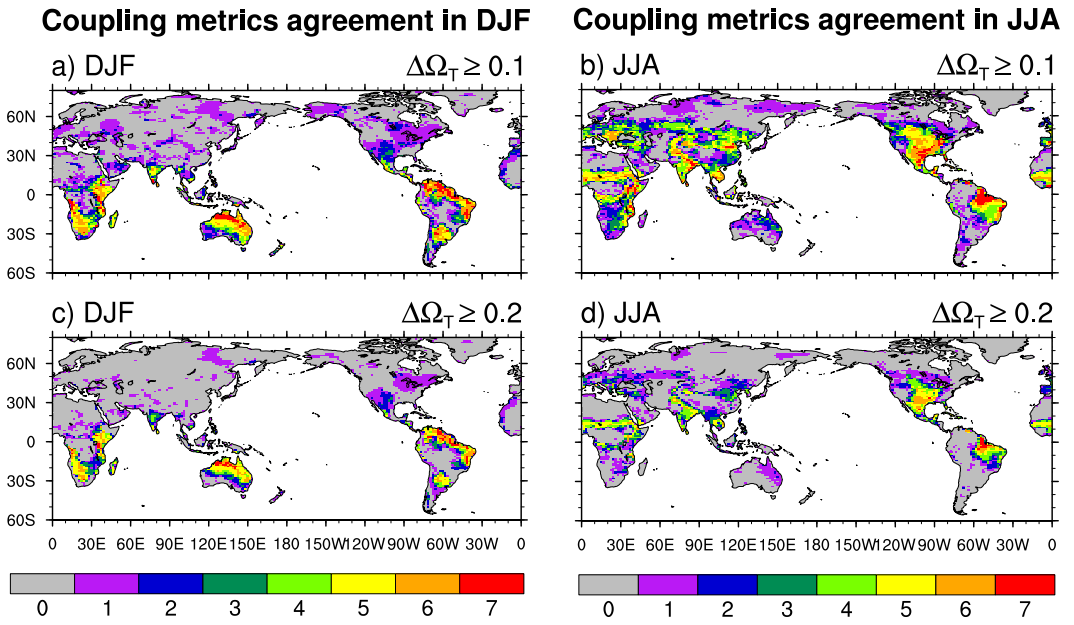

FIG. 12. Agreement between the different coupling measures $\Delta\Omega_T$, $\Delta\Omega_{T,\mathrm{GCCMIP5}}$, variance analysis, correlation (ET, T), Π, $I_{\mathrm{SM}-T}$, and the 90th quantile regression slope. Variable $\Delta\Omega_T$ is chosen to be (a),(b) ≥0.1 for strongly coupled or (c),(d) ≥0.2 for very strongly coupled. For $\Delta\Omega_{T,\mathrm{GCCMIP5}}$, variance analysis, correlation(ET, T), Π, $I_{\mathrm{SM}-T}$, and the 90th quantile regression slope, the threshold was chosen so the same fraction of land area is above the $\Delta\Omega_T$ GLACE-1 thresholds. The resulting thresholds are shown in Table 1.

disagree on the location of strong land–atmosphere coupling.

The importance of a possible trend in defining land–atmosphere coupling strength is consistent with Seneviratne et al. (2013) but is also worrisome. An increasing amount of evidence points to coupling strength affecting the simulation of heat waves and other extreme events (Fischer et al. 2007; Koster et al. 2009b; Hirschi et al. 2011; Mueller and Seneviratne 2012; Miralles et al. 2014). It follows that changes in coupling strength, linked to possible soil moisture trends, would therefore affect model projections in these extremes. Unfortunately, the soil moisture projections are uncertain and, we suspect, differ between the CMIP5 models. Strong and very strong land–atmosphere coupling is a regional feature, and trends in soil moisture at these scales are linked to a range of phenomena that are challenging for climate models to resolve (see Pitman et al. 2012), including how soil moisture is represented in climate models. In short, the detailed pattern of how coupling strength will change through the twenty-first century depends on the complex interrelationship between the land and the atmosphere. This contributes significant additional uncertainty in the simulation of future extremes at scales of significance for climate change adaptation.

5. Conclusions

We have investigated the coupling strength of ACCESS1.3b by examining different land–atmosphere coupling measures obtained from GLACE-1 and GLACE-CMIP5 experiments. We showed that ACCESS1.3b land–atmosphere coupling strength was in the range previously reported by other models. We therefore conclude that it is unlikely that the biases identified in the performance of ACCESS1.3b by Lorenz et al. (2014) relate to an anomalous coupling strength.

We identified differences in land–atmosphere coupling strength between the Northern and Southern Hemisphere summers. The Southern Hemisphere summer was more strongly coupled, with larger values in $\Delta\Omega$ for temperature. Overall, the Southern Hemisphere appears to behave differently than the Northern Hemisphere, where the hot spots occur in regions between wet and dry climates. The Southern Hemisphere was most strongly coupled in the tropics and in the midlatitudes. Whether this result is specific to ACCESS1.3b will require experiments with other models to be undertaken.

Of more general significance, we have shown that different land–atmosphere coupling measures agree on the location of very strongly coupled regions, but agree less for intermediate and weakly coupled regions. The $\Delta\Omega_T$ from GLACE-1 and GLACE-CMIP5,

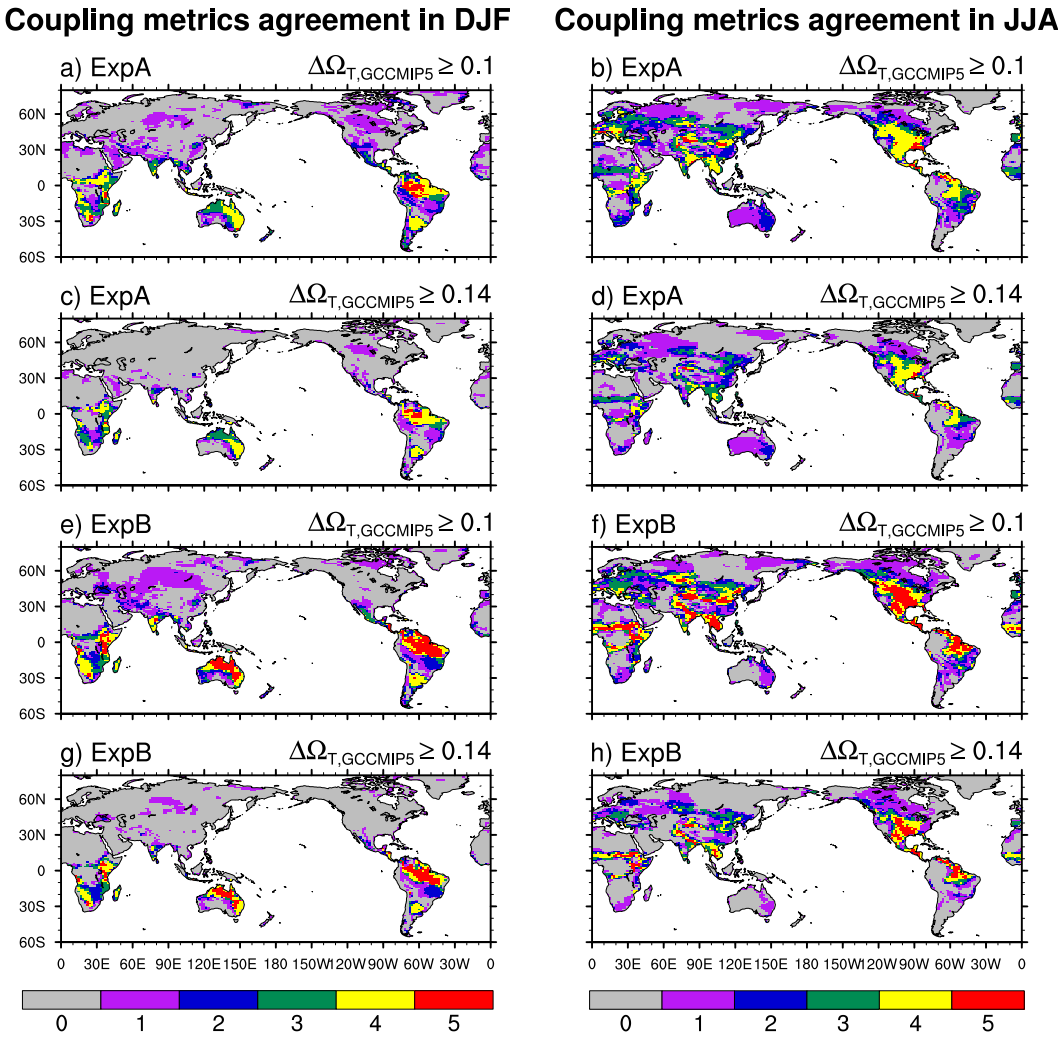

FIG. 13. Agreement between different coupling metrics $\Delta\Omega_{T,\mathrm{GCCMIP5}}$, variance analysis, correlation(ET, T), Π, and $I_{\mathrm{SM}-T}$ for (a)–(d) ExpA and (e)–(h) ExpB during 2080–2100. We used the averages of the thresholds for strongly coupled so that the same fraction of land area is above the threshold (0.1 or 0.2) as for $\Delta\Omega_T$ GLACE-1 in present climate (Table 1) during (left) DJF and (right) JJA.

even though obtained over different time scales, are strongly linked and provide similar information. There is no clear relationship between the other measures unless they can be scaled. If scaled, these other measures then lead to very similar spatial results as GLACE-1 and GLACE-CMIP5. Unfortunately, this suggests that specific coupling experiments, like GLACE-1 or GLACE-CMIP5, are required to obtain consistent measures of coupling strength or to obtain an idea about how the different measures scale in a particular climate model. We do note, however, that there appears to be general agreement across the measures in identifying regions with very strong coupling.

Last, we showed that if a model simulates a soil moisture trend, this largely determines the soil moisture–atmosphere coupling at the end of the twenty-first century. We therefore conclude that unless a model captures the right trend (if indeed a trend occurs) in soil moisture in climate projections, changes in land–atmosphere coupling will be under- or overestimated for future projections. This would tend to lead to major biases in atmospheric variables, especially mean and maximum temperature, and perhaps significant biases in the simulation of some land-associated extremes such as droughts and heatwaves.

Acknowledgments. This study was supported by the Australian Research Council (CE110001028) and the NCI National Facility at the ANU. We thank Sonia Seneviratne for help with the coupling measures and for

fruitful discussions. We also thank Gab Abramowitz and Agus Santoso. We thank the two anonymous reviewers for their helpful comments and feedback which significantly improved the manuscript.

REFERENCES

Betts, A. K., J. H. Ball, A. C. M. Beljaars, M. J. Miller, and P. A. Viterbo, 1996: The land surface–atmosphere interaction: A review based on observational and global modelling perspectives. *J. Geophys. Res.*, **101**, 7209–7225, doi:10.1029/95JD02135.

Bi, D., and Coauthors, 2013: The ACCESS coupled model: Description, control climate and evaluation. *Aust. Meteor. Oceanogr. J.*, **63**, 9–32.

Boberg, F., and J. H. Christensen, 2012: Overestimation of Mediterranean summer temperature projections due to model deficiencies. *Nat. Climate Change*, **2**, 433–436, doi:10.1038/nclimate1454.

CPC, 2013a: Monthly OISST.v2 (1981–2010 base period) data. NOAA/NWS/CPC, accessed 12 May 2013. [Available online at http://www.cpc.ncep.noaa.gov/data/indices/sstoi.indices.]

——, 2013b: Monthly OISST.v1 (1971–2000 base period) data. NOAA/NWS/CPC, accessed 12 May 2013. [Available online at http://www.cpc.ncep.noaa.gov/data/indices/old_indices/sstoi.indices_old.]

Davies, T., M. J. P. Cullen, A. J. Malcolm, M. H. Mawson, A. Staniforth, A. A. White, and N. Wood, 2005: A new dynamical core for the Met Office's global and regional modelling of the atmosphere. *Quart. J. Roy. Meteor. Soc.*, **131**, 1759–1782, doi:10.1256/qj.04.101.

Delworth, T. L., and S. Manabe, 1988: The influence of potential evaporation on the variabilities of simulated soil wetness and climate. *J. Climate*, **1**, 523–547, doi:10.1175/1520-0442(1988)001<0523:TIOPEO>2.0.CO;2.

Diffenbaugh, N. S., and M. Ashfaq, 2010: Intensification of hot extremes in the United States. *Geophys. Res. Lett.*, **37**, L15701, doi:10.1029/2010GL043888.

Dirmeyer, P. A., 2011: The terrestrial segment of soil moisture–climate coupling. *Geophys. Res. Lett.*, **38**, L16702, doi:10.1029/2011GL048268.

——, Y. Jin, B. Singh, and X. Yan, 2013a: Evolving land–atmosphere interactions over North America from CMIP5 simulations. *J. Climate*, **26**, 7313–7327, doi:10.1175/JCLI-D-12-00454.1.

——, ——, ——, and ——, 2013b: Trends in land–atmosphere interactions from CMIP5 simulations. *J. Hydrometeor.*, **14**, 829–849, doi:10.1175/JHM-D-12-0107.1.

——, Z. Wang, M. J. Mbuh, and H. E. Norton, 2014: Intensified land surface control on boundary layer growth in a changing climate. *Geophys. Res. Lett.*, **41**, 1290–1294, doi:10.1002/2013GL058826.

Dix, M., and Coauthors, 2013: The ACCESS coupled model: Documentation of core CMIP5 simulations and initial results. *Aust. Meteor. Oceanogr. J.*, **63**, 83–99.

Edwards, J., and A. Slingo, 1996: Studies with a flexible new radiation code. I: Choosing a configuration for a large-scale model. *Quart. J. Roy. Meteor. Soc.*, **122**, 689–719, doi:10.1002/qj.49712253107.

Findell, K. L., and E. A. B. Eltahir, 2003: Atmospheric controls on soil moisture boundary layer interactions. Part II: Feedbacks within the continental United States. *J. Hydrometeor.*, **4**, 570–583, doi:10.1175/1525-7541(2003)004<0570:ACOSML>2.0.CO;2.

Fischer, E. M., S. I. Seneviratne, D. Lüthi, and C. Schär, 2007: Contribution of land–atmosphere coupling to recent European summer heat waves. *Geophys. Res. Lett.*, **34**, L06707, doi:10.1029/2006GL029068.

Flato, G., and Coauthors, 2013: Evaluation of climate models. *Climate Change 2013: The Physical Science Basis*, T. F. Stocker et al., Eds., Cambridge University Press, 741–866.

Ford, T. W., and S. M. Quiring, 2014: In situ soil moisture coupled with extreme temperatures: A study based on the Oklahoma Mesonet. *Geophys. Res. Lett.*, **41**, 4727–4734, doi:10.1002/2014GL060949.

Gates, W. L., 1992: AMIP: The Atmospheric Model Intercomparison Project. *Bull. Amer. Meteor. Soc.*, **73**, 1962–1970, doi:10.1175/1520-0477(1992)073<1962:ATAMIP>2.0.CO;2.

Gregory, D., and P. Rowntree, 1990: A mass flux convection scheme with representation of cloud ensemble characteristics and stability-dependent closure. *Mon. Wea. Rev.*, **118**, 1483–1506, doi:10.1175/1520-0493(1990)118<1483:AMFCSW>2.0.CO;2.

Guo, Z., and P. A. Dirmeyer, 2013: Interannual variability of land–atmosphere coupling strength. *J. Hydrometeor.*, **14**, 1636–1646, doi:10.1175/JHM-D-12-0171.1.

Hewitt, H. T., D. Copsey, I. D. Culverwell, C. M. Harris, R. S. R. Hill, A. B. Keen, A. J. McLaren, and E. C. Hunke, 2011: Design and implementation of the infrastructure of HadGEM3: The next-generation Met Office climate modelling system. *Geosci. Model Dev.*, **4** (2), 223–253, doi:10.5194/gmd-4-223-2011.

Hirsch, A. L., J. Kala, A. J. Pitman, C. Carouge, J. P. Evans, V. Haverd, and D. Mocko, 2014a: Impact of land surface initialization approach on subseasonal forecast skill: A regional analysis in the Southern Hemisphere. *J. Hydrometeor.*, **15**, 300–319, doi:10.1175/JHM-D-13-05.1.

——, A. J. Pitman, S. I. Seneviratne, J. P. Evans, and V. Haverd, 2014b: Summertime maximum and minimum temperature coupling asymmetry over Australia determined using WRF. *Geophys. Res. Lett.*, **41**, 1546–1552, doi:10.1002/2013GL059055.

Hirschi, M., and Coauthors, 2011: Observational evidence for soil-moisture impact on hot extremes in southeastern Europe. *Nat. Geosci.*, **4**, 17–21, doi:10.1038/ngeo1032.

Jaeger, E. B., and S. I. Seneviratne, 2011: Impact of soil moisture–atmosphere coupling on European climate extremes and trends in a regional climate model. *Climate Dyn.*, **36**, 1919–1939, doi:10.1007/s00382-010-0780-8.

Koster, R. D., P. A. Dirmeyer, A. N. Hahmann, R. Ijpelaar, L. Tyahla, P. M. Cox, and M. J. Suarez, 2002: Comparing the degree of land–atmosphere interaction in four atmospheric general circulation models. *J. Hydrometeor.*, **3**, 363–375, doi:10.1175/1525-7541(2002)003<0363:CTDOLA>2.0.CO;2.

——, and Coauthors, 2004: Regions of strong coupling between soil moisture and precipitation. *Science*, **305**, 1138–1140, doi:10.1126/science.1100217.

——, and Coauthors, 2006: GLACE: The Global Land–Atmosphere Coupling Experiment. Part I: Overview. *J. Hydrometeor.*, **7**, 590–610, doi:10.1175/JHM510.1.

——, S. D. Schubert, and M. J. Suarez, 2009a: Analyzing the concurrence of meteorological droughts and warm periods, with implications for the determination of evaporative regime. *J. Climate*, **22**, 3331–3341, doi:10.1175/2008JCLI2718.1.

——, H. Wang, S. D. Schubert, M. J. Suarez, and S. Mahanama, 2009b: Drought-induced warming in the continental United States under different SST regimes. *J. Climate*, **22**, 5385–5400, doi:10.1175/2009JCLI3075.1.

——, and Coauthors, 2011: The second phase of the Global Land–Atmosphere Coupling Experiment: Soil moisture contributions to subseasonal forecast skill. *J. Hydrometeor.*, **12**, 805–822, doi:10.1175/2011JHM1365.1.

Kowalczyk, E. A., and Coauthors, 2013: The land surface model component of ACCESS: Description and impact on the simulated surface climatology. *Aust. Meteor. Oceanogr. J.*, **63**, 65–82.

Lewis, S. C., and D. J. Karoly, 2013: Evaluation of historical diurnal temperature range trends in CMIP5 models. *J. Climate*, **26**, 9077–9089, doi:10.1175/JCLI-D-13-00032.1.

Lorenz, R., E. L. Davin, and S. I. Seneviratne, 2012: Modeling land–climate coupling in Europe: Impact of land surface representation on climate variability and extremes. *J. Geophys. Res.*, **117**, D20109, doi:10.1029/2012JD017755.

——, A. J. Pitman, M. G. Donat, A. L. Hirsch, J. Kala, E. A. Kowalczyk, R. M. Law, and J. Srbinovsky, 2014: Representation of climate extreme indices in the ACCESS1.3b coupled atmosphere–land surface model. *Geosci. Model Dev.*, **7**, 545–567, doi:10.5194/gmd-7-545-2014.

Martin, G. M., M. A. Ringer, V. D. Pope, A. Jones, C. Dearden, and T. J. Hinton, 2006: The physical properties of the atmosphere in the New Hadley Centre Global Environmental Model (HadGEM1). Part I: Model description and global climatology. *J. Climate*, **19**, 1274–1301, doi:10.1175/JCLI3636.1.

Miralles, D. G., M. J. van den Berg, A. J. Teuling, and R. A. M. de Jeu, 2012: Soil moisture–temperature coupling: A multiscale observational analysis. *Geophys. Res. Lett.*, **39**, L21707, doi:10.1029/2012GL053703.

——, A. J. Teuling, C. C. van Heerwaarden, and J. Vilà-Guerau de Arellano, 2014: Mega-heatwave temperatures due to combined soil desiccation and atmospheric heat accumulation. *Nat. Geosci.*, **7**, 345–349, doi:10.1038/ngeo2141.

Mueller, B., and S. I. Seneviratne, 2012: Hot days induced by precipitation deficits at the global scale. *Proc. Natl. Acad. Sci. USA*, **109**, 12 398–12 403, doi:10.1073/pnas.1204330109.

——, and ——, 2014: Systematic land climate and evapotranspiration biases in CMIP5 simulations. *Geophys. Res. Lett.*, **41**, 128–134, doi:10.1002/2013GL058055.

Orlowsky, B., and S. I. Seneviratne, 2010: Statistical analyses of land–atmosphere feedbacks and their possible pitfalls. *J. Climate*, **23**, 3918–3932, doi:10.1175/2010JCLI3366.1.

PCMDI, 2013: AMIP boundary condition data at 1 by 1 degree resolution. Lawrence Livermore National Laboratory, accessed 17 July 2013. [Available online at http://www-pcmdi.llnl.gov/projects/amip/AMIP2EXPDSN/BCS/amipbc_dwnld.php.]

Pitman, A. J., A. Arneth, and L. Ganzeveld, 2012: Regionalizing global climate models. *Int. J. Climatol.*, **32**, 321–337, doi:10.1002/joc.2279.

Priestley, C. H. B., and R. J. Taylor, 1972: On the assessment of surface heat flux and evaporation using large-scale parameters. *Mon. Wea. Rev.*, **100**, 81–92, doi:10.1175/1520-0493(1972)100<0081:OTAOSH>2.3.CO;2.

Puri, K., and Coauthors, 2013: Implementation of the initial ACCESS numerical weather prediction system. *Aust. Meteor. Oceanogr. J.*, **63**, 265–284.

Quesada, B., R. Vautard, P. Yiou, M. Hirschi, and S. I. Seneviratne, 2012: Asymmetric European summer heat predictability from wet and dry southern winters and springs. *Nat. Climate Change*, **2**, 736–741, doi:10.1038/nclimate1536.

Seneviratne, S. I., D. Lüthi, M. Litschi, and C. Schär, 2006: Land–atmosphere coupling and climate change in Europe. *Nature*, **443**, 205–209, doi:10.1038/nature05095.

——, T. Corti, E. L. Davin, M. Hirschi, E. B. Jaeger, I. Lehner, B. Orlowsky, and A. J. Teuling, 2010: Investigating soil moisture–climate interactions in a changing climate: A review. *Earth-Sci. Rev.*, **99**, 125–161, doi:10.1016/j.earscirev.2010.02.004.

——, and Coauthors, 2013: Impact of soil moisture–climate feedbacks on CMIP5 projections: First results from the GLACE-CMIP5 experiment. *Geophys. Res. Lett.*, **40**, 5212–5217, doi:10.1002/grl.50956.

Taylor, K. E., D. Williamson, and F. Zwiers, 2000: The Sea Surface Temperature and Sea-Ice Concentration Boundary Conditions For AMIP II Simulations. PCMDI Rep. 60, 24 pp. [Available online at http://www-pcmdi.llnl.gov/publications/pdf/60.pdf.]

van den Hurk, B., F. Doblas-Reyes, G. Balsamo, R. D. Koster, S. I. Seneviratne, and H. Camargo Jr., 2012: Soil moisture effects on seasonal temperature and precipitation forecast scores in Europe. *Climate Dyn.*, **38**, 349–362, doi:10.1007/s00382-010-0956-2.

Wang, G., Y. Kim, and D. Wang, 2007: Quantifying the strength of soil moisture–precipitation coupling and its sensitivity to changes in surface water budget. *J. Hydrometeor.*, **8**, 551–570, doi:10.1175/JHM573.1.

Wang, Y. P., and R. Leuning, 1998: A two-leaf model for canopy conductance, photosynthesis and partitioning of available energy I: Model description and comparison with a multi-layered model. *Agric. For. Meteor.*, **91**, 89–111, doi:10.1016/S0168-1923(98)00061-6.

——, E. Kowalczyk, R. Leuning, G. Abramowitz, M. R. Raupach, B. Pak, E. van Gorsel, and A. Luhar, 2011: Diagnosing errors in a land surface model (CABLE) in the time and frequency domains. *J. Geophys. Res.*, **116**, G01034, doi:10.1029/2010JG001385.

Zhang, X., L. Alexander, G. C. Hegerl, P. Jones, A. K. Tank, T. C. Peterson, B. Trewin, and F. W. Zwiers, 2011: Indices for monitoring changes in extremes based on daily temperature and precipitation data. *Wiley Interdiscip. Rev.: Climate Change*, **2**, 851–870, doi:10.1002/wcc.147.